Biophysical Chemistry 172 (2013) 26–36

Contents lists available at SciVerse ScienceDirect

Biophysical Chemistry

journal homepage: http://www.elsevier.com/locate/biophyschem

Aggregation of anti-streptavidin immunoglobulin gamma-1 involves Fab unfolding and competing growth pathways mediated by pH and salt concentration

Nayoung Kim [a], Richard L. Remmele Jr. [b,1], Dingjiang Liu [b,2], Vladimir I. Razinkov [c], Erik J. Fernandez [d], Christopher J. Roberts [a,*]

[a] Department of Chemical and Biomolecular Engineering, University of Delaware, Newark, DE 19716, United States
[b] Drug Product Development, Amgen Inc., Thousand Oaks, CA 91320, United States
[c] Drug Product Development, Amgen Inc., Seattle, WA 98119, United States
[d] Department of Chemical Engineering, University of Virginia, Charlottesville, VA 22904, United States

HIGHLIGHTS

- Aggregation of anti-SA IgG1 involves Fab unfolding to initiate dimer and soluble aggregate formation.
- Aggregate growth pathways are mediated by electrostatic interactions between aggregates.
- pH and [NaCl] mediate aggregate–aggregate coalescence and phase behavior with a pattern more general for other proteins.
- Conformational changes detected by different spectroscopic techniques appear to be less easily generalized.

GRAPHICAL ABSTRACT

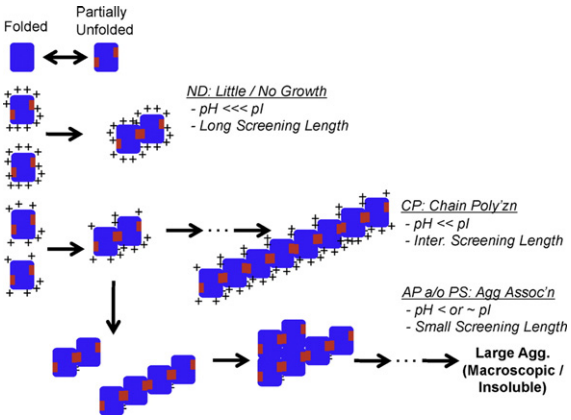

ARTICLE INFO

Article history:
Received 19 August 2012
Received in revised form 29 November 2012
Accepted 18 December 2012
Available online 26 December 2012

Keywords:
Antibody
Aggregation
Unfolding
Protein interaction

ABSTRACT

Changes in non-native aggregation mechanisms of an anti-streptavidin (anti-SA) IgG1 antibody were determined over a wide range of pH and [NaCl] under accelerated (high temperature) conditions, using a combination of calorimetry, chromatography, static light scattering, dye binding, and spectroscopy (fluorescence, infra-red, and circular dichroism). Aggregation rates were strongly influenced by conformational stability of at least the Fab regions, but were only weakly affected by changes in electrostatic colloidal interactions. This was in contrast to the effects of electrostatic interactions on aggregate growth, as the dominant growth mechanism shifted dramatically with pH and [NaCl]. Pre-formed aggregates also displayed a reversible cloud-point boundary that quantitatively aligned with the overall pattern of aggregation mechanisms as a function of pH and [NaCl], suggesting an underlying thermodynamic transition may dictate whether molecular aggregates will coalesce into macroscopic particles. Structural changes upon unfolding and aggregation were also sensitive to pH and [NaCl]. Interestingly, Thioflavin T binding was essentially indistinguishable for

* Corresponding author. Tel./fax: +1 302 831 0838.
E-mail address: cjr@udel.edu (C.J. Roberts).
[1] Current address: MedImmune, 319 Bernardo Avenue, Mountain View, CA 94043, United States.
[2] Current address: Formulation Development, Regeneron Pharmaceuticals Inc., Tarrytown, NY 10590, United States.

0301-4622/$ – see front matter
http://dx.doi.org/10.1016/j.bpc.2012.12.004

aggregates formed in different pH and [NaCl] conditions, however, the other assays indicated notable differences across different solvent conditions. This suggests that the overall degree of conformational change during aggregation can be influenced by electrostatic interactions, but suggests caution in interpreting whether available techniques detect changes that are directly relevant to the mechanism(s) of aggregate formation and growth.

1. Introduction

Monoclonal antibodies (mAbs) are an increasingly important class of biotechnology products, due to their relatively specific interactions and utility in many applications, such as treating and diagnosing diseases, and more generally as biochemical diagnostic tools [1,2]. As with other protein-based biotechnology products, antibodies are prone to both chemical and physical degradation pathways, of which non-native aggregation is among the most common [3]. Aggregation must be minimized in the final product for a variety of reasons. Aggregates may lead to loss of efficacy in the final product, and impact marketability for pharmaceutical products [4,5]. In addition, aggregates raise concerns regarding possible immunogenic responses for therapeutic proteins [6–9]. It has been suggested that the severity and type of immunogenic response (if any) for protein aggregates depends on the amount, size, and type of aggregate in solution [10,11].

Nonnative aggregation can occur at many of the steps in the development of protein products, at least in part because a number of different stresses can promote aggregate formation. These include: [3,4,12] low pH needed for viral inactivation of pharmaceuticals; elevated temperatures; freezing and thawing of bulk solutions; contact with different materials used in manufacturing, storage, or delivery devices; and agitation. Any of these stresses can, in principle, increase the population of partially or fully unfolded monomers that are often implicated as key intermediates along non-native aggregation pathways [10,13–16].

Once formed, non-native aggregates (hereafter simply referred to as aggregates) are typically irreversible under the conditions in which they were created, and require extreme sample conditions to dissociate them — for example, concentrated chemical denaturants or high pressure [16,17]. This may be due, at least in part, to conformational changes that accompany aggregation. Aggregates of many proteins have been found to contain increased amounts of intermolecular beta sheet structures [14,16,18–20], although it is not always clear how much or what particular structural changes are required within a given protein in order to facilitate aggregation [1].

In bulk solution, important solvent variables include pH, ionic strength, salt or buffer type, and the presence and concentration of different excipients. At a minimum, changes to any of these variables can affect protein conformational stability and/or protein–protein interactions [16,21–23,30,31]. In addition to the rate of aggregation, these variables can also influence the mechanism of aggregation, and possibly then the resulting aggregate structure, size, and/or morphology.

Prior work has demonstrated that changes in solvent conditions can cause the same protein to form aggregates of different sizes, morphologies, and/or underlying secondary structures. Li et al. [24] showed that the mechanism of aggregate growth varied as a function of pH and [NaCl] for a globular protein, alpha-Chymotrypsinogen A (aCgn), with electrostatic repulsions between aggregates playing an important role in biasing towards different mechanisms [24]. Similarly, alpha-Synucleincan aggregate to form different morphologies, depending on the solution pH and salt concentration; [25] as can beta-lactoglobulin [18]. These studies empirically show that pH and ionic strength can strongly influence the qualitative characteristics of aggregates that form over time.

For selected conditions, IgG1 and IgG2 antibodies [26,11,27] have previously been shown to switch aggregate growth pathways based on changes in pH, and to a some extent based on solution ionic strength. The present work, to the best of our knowledge, includes the most systematic report to date of the global aggregation behavior and mechanisms of an IgG1 across a broad range of pH and [NaCl] conditions that are relevant to therapeutic protein products. In addition, the phase behavior of aggregates of anti-SA IgG1 is characterized in terms of cloud points, analogous to what has been shown recently for aCgn, and in less detail for a different IgG1 and an IgG2 [26,28,29].

The protein used here is anti-streptavidin (anti-SA) IgG1. In prior work, it was shown that this molecule is aggregation prone, albeit somewhat less so than its IgG2 version [33], with aggregation accelerated by exposure to elevated temperature, stainless steel [34], or high levels of silicone oil and/or agitation [35]. In this report, factors influencing the mechanism(s) of aggregation were experimentally characterized as a function of pH and [NaCl] under accelerated (elevated temperature) conditions. The results highlight the importance of competing effects of protein conformational stability and protein–protein interactions, as well as difficulties regarding the use of common structural assays to assess the conformational changes that are important for mitigating aggregation. Comparison to recent reports for other proteins over a broad range of pH and [NaCl] illustrates that while some aspects of aggregation mechanisms may be highly protein specific, some aspects show promise of generalization based on established biophysical considerations.

2. Materials and methods

Purified anti-streptavidin (anti-SA) IgG1 antibody was provided by Amgen as a stock solution (approx. 30 mg/mL protein). The purities of all stock solutions were confirmed to be greater than 98% monomer by peak area in size-exclusion chromatography, with the only other detectable species being dimer (see also below). Buffer preparation was as described previously [11]. Protein samples were doubly dialyzed against a given buffer using Spectra/Por 7 dialysis tubing (10,000 Da molecular weight cutoff, Spectrum Laboratories, Rancho Dominguez, California) and filtered (0.22 μm syringe filters). Post-dialysis protein concentration was determined using absorbance at 280 nm measured with a UV–Vis spectrophotometer (Agilent 8453 UV–Vis; Agilent Technologies, Santa Clara, CA). Final protein concentration was adjusted gravimetrically, as needed, using the corresponding dialysis buffer. Size exclusion chromatography (SEC) and differential scanning calorimetry (DSC) measurements were conducted as described previously, as was analysis of the data [10,26,36,38,39]. Additional details regarding SEC and inline multi-angle light scattering are provided in Supplementary information.

2.1. Aggregation half life versus temperature

The temperature at which the half life for monomer loss was 2 h (protein concentration = 1 mg/mL) was determined as a function of pH and NaCl concentration, using the methods described in Supporting Information [40,41]. This corresponds to the point at which the fraction of initial monomer (m, defined as monomer concentration scaled by initial concentration) is 0.5 for a sample incubated for 2 h.

2.2. Static light scattering (SLS) to assess colloidal monomer interactions

Static light scattering experiments were performed as described previously [11,29]. Averaged scattered intensities were confirmed as independent of scattering angle (not shown) and converted to excess

Rayleigh ratios (R_{ex}) using toluene as a reference, as described previously [11]. R_{ex} as a function of protein concentration (c) was regressed using Eq. (1) to determine values of the apparent molecular weight (M_w) and protein–protein Kirkwood Buff integral (G_{22}) [42] for each solvent condition tested.

$$\frac{R_{ex}}{K} = M_w c + G_{22} c. \quad (1)$$

2.3. [NaCl]–pH state diagram

Concentrated stock protein solutions were prepared by dialysis against 5 mM sodium citrate buffers at pH 4, 5, or 6. After dialysis, protein stock solutions were diluted to 1 mg/mL using a combination of the dialysis buffer and a corresponding buffer in which 2 M NaCl was dissolved. The stock protein solution and the buffers, with and without added NaCl, were combined gravimetrically to reach the desired concentration of NaCl. Because NaCl was added after pH adjustment, in some cases this resulted in final pH values (tested independently) that were slightly lower than samples without added NaCl, due to shifts in buffer pKa at high ionic strengths.

A state diagram was constructed by categorizing what type of aggregation mechanism was observed, as a function of pH and added NaCl, during isothermal aggregation at elevated temperatures similar to those determined from response surface of $T_{2\,h}$ as a function of pH and [NaCl]. Aggregation was monitored by SEC–MALS and visible observation as a function of incubation time at elevated temperatures; particular temperature values were chosen as a function of pH and [NaCl] so as to keep experimental time scales less than a few hours to achieve one to two half lives of monomer loss. After quenching in an ice-water bath, each sample was centrifuged at nominally 10,000 *g* for a minimum of 5 min to remove any insoluble aggregates from solution, and the supernatant was assayed on SEC–MALS as described above. Samples were stored and monitored (SEC–MALS and visible observation) under refrigerated conditions to confirm that no detectable dissociation or further aggregation occurred on time scales of days, after initial incubation at elevated temperature.

2.4. pH titrations for pre-formed aggregates

Cloud points for otherwise soluble aggregates were determined based on pH titration with small volumes of concentrated base and/or acid, using methods described previously [26,28]. Additional details are provided in Supporting information.

2.5. Far-UV circular dichroism (CD)

Far-UV circular dichroism (CD) was used to assess the average secondary structure of aggregated samples and monomer controls at selected solution conditions, summarized in Table S1 of Supporting information. Additional details are as described elsewhere [10]. The mean residue ellipticity values (MRE_{tot}) are reported after first subtracting the monomer contribution, and normalizing on a per-unit-mass of aggregate to obtain the aggregate spectra (MRE_{agg}).

$$MRE_{agg} = \frac{MRE_{tot} - m \times MRE_{mon}}{(1-m)}. \quad (2)$$

The m values were from SEC for a given for sample, and MRE_{mon} is the corresponding CD spectrum of the monomer control.

2.6. Intrinsic fluorescence

Structural changes with aggregation were evaluated using intrinsic fluorescence for the same conditions as for CD spectroscopy. Methods were otherwise as described previously [10]. The monomer contributions to the aggregate emission spectra were subtracted, and then the spectra normalized on an aggregate mass basis, using Eq. (2) but replacing *MRE* with the fluorescence intensity at a given wavelength within the spectrum.

2.7. Thioflavin T binding

Thioflavin T (ThT) binding was measured for the same samples as described in the preceding subsections, using the fluorescence instrumentation described above, and methods described previously [10,11]. Residual monomer contributions for each ThT emission spectrum were subtracted in an analogous manner to that described above (cf. Eq. (2)).

2.8. Fourier-transform infrared (FTIR) spectroscopy

Secondary structure analysis by infrared spectroscopy was performed using a Vertex 70 spectrometer (BrukerOptik GmbH, Ettlingen, Germany) with an LN-MCT liquid nitrogen-cooled detector purged with dry air, and with a BioATR-II multiple-reflection horizontal ATR (attenuated total reflectance) accessory held at room temperature. Spectra were collected using Bruker OPUS software through averaging of 256 spectral accumulations for each sample over the range 1000 to 4000 cm^{-1} (resolution = 4 cm^{-1}), and corrected for baseline and normalized.

3. Results

3.1. Conformational stability by differential scanning calorimetry (DSC)

Relative conformational stability of anti-SA IgG1 monomer was characterized as a function of pH and added NaCl via DSC, with the excess heat capacity versus temperature (T) shown in Fig. 1. As expected from previous studies on the unfolding of an IgG1 [44,45], DSC scans showed a maximum of three unfolding events. At pH 4, the unfolding of each of the domains (Fab, C_H2, and C_H3) appeared distinguishably as three individual endotherms with the second peak having the largest area. At pH 5 and 6, only one peak was obvious, with possibly a shoulder towards lower T for pH 5 conditions. At high temperatures, the aggregates precipitated at these higher pH conditions, resulting in strong exotherms in the thermo grams (see Fig. 1). The pI of this IgG is approximately 9, and therefore as pH changes from 4 to 6 it is expected that the net charge on the protein is decreasing (see also Discussion section).

For conditions where more than one peak was clearly distinguishable (pH 4), partial DSC scans were performed to determine reversibility of the unfolding events, using the same sample to repeatedly heat to successively higher T values. As shown in Supporting information (Fig. S2), the first endotherm was reversible, while the second peak was not reversible to a significant degree, and showed signs of aggregation upon rescanning, in that once the second transition was scanned partially, a subsequent scan showed a greatly reduced endotherm (cf. dashed curve and solid gray curve in Fig. S2). Samples that were scanned to these temperatures and then quenched and analyzed by SEC also clearly showed no monomer loss for heating up to the start of the second endotherm, but dramatic loss once the second transition region was accessed (data not shown). The magnitude and location of the endotherm for the third transition was not significantly affected by the previous heating scans. This pattern in similar to that seen previously for other IgGs [46,47].

According to previous studies on the conformational stability of IgG1s, the first, smaller peak is likely the unfolding of the C_H2 domain, and the second, larger peak is the unfolding of the Fab domain [44,45] at these acidic pH values; with the smaller peak at the highest temperature range corresponding to the C_H3 domain [44,45]. This would indicate that C_H2 unfolding is not sufficient to cause non-native

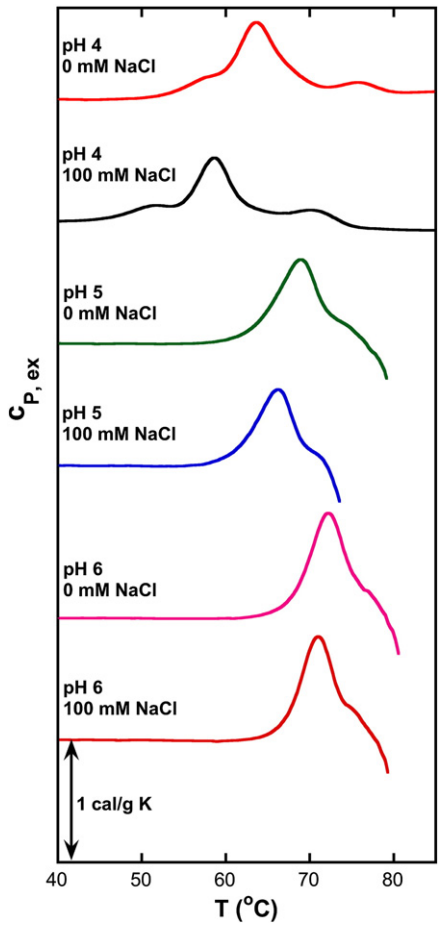

Fig. 1. Excess heat capacity from differential scanning calorimetry (DSC). The initial linear behavior of the c_P versus temperature was taken as the (extrapolated) native monomer baseline, and this was subtracted out from the absolute c_P to calculate the $c_{P,ex}$.

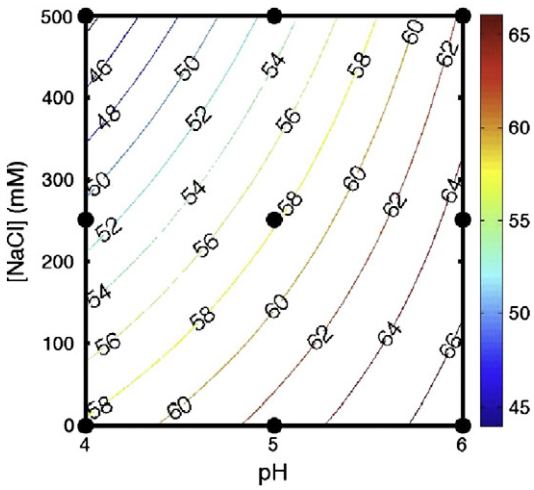

Fig. 2. Contour plot of $T_{2\,h}$ (indicated by labels and color code) as a function of pH and added NaCl concentration based on a face-centered cubic response-surface DOE (see main text and Supporting information for additional details). Labels on the curves indicate the temperature for a given contour.

aggregation at these conditions and time scales, but Fab unfolding is required. It is not possible to discern from these data whether Fc unfolding may be involved at much lower temperatures where much longer time scales for aggregation can be accessed (see also, Discussion). At higher pH values, there was only one visibly discernable endotherm, and this was irreversible in all cases based on a single DSC rescan (not shown).

3.2. $T_{2\,h}$ and aggregation rates versus pH and [NaCl]

The relative rates of aggregation as a function of pH and NaCl concentration were quantified through a response surface via statistical design of experiments (DOE) [48]. The response variable in this case was $T_{2\,h}$, the interpolated temperature at which the half-life for monomer loss is 2 h. $T_{2\,h}$ was chosen because it is a relatively quick method to compare the rates of aggregation among conditions that have widely varying half-lives as a function of temperature, anywhere from seconds to weeks, across the full set of pH and [NaCl] of interest. Higher $T_{2\,h}$ values correspond to longer half-lives if the aggregation reactions were carried out at the same temperature across the different conditions. $T_{2\,h}$ values were determined at the particular pH and [NaCl] values indicated by the filled black circles Fig. 2. Additional details are given in Supporting information.

Fig. 2 shows the response surface contour plot of $T_{2\,h}$ as a function of pH and [NaCl]. $T_{2\,h}$ varied between 44 °C and 66 °C in the experimental-design space. The lowest $T_{2\,h}$ value was at the lowest pH and highest NaCl concentration, while the highest $T_{2\,h}$ value was at the highest pH and lowest NaCl concentration. This indicates that increasing pH (towards the pI) and increasing salt concentration have opposite effects on $T_{2\,h}$, and thus on the relative rates of aggregation. The relative spacing between the isotherms in the contour plot indicates that the aggregation rates are more sensitive to changing [NaCl] (with fixed pH) at low pH, with a shift of ~14 °C from lowest to highest [NaCl] at pH 4, compared to a shift of ~5 °C at pH 6.

3.3. Colloidal interactions by static light scattering (SLS)

Static light scattering (SLS) was implemented to study the effects of pH and added NaCl on the net colloidal interactions between native monomers at room temperature. The SLS data were analyzed using Eq. (1) (see Materials and methods) based on the model developed by Blanco et al., which shows that the protein–protein Kirkwood–Buff (KB) integral, G_{22}, is a more relevant measure of net colloidal interactions obtainable from light scattering than the traditional second osmotic virial coefficient (B_{22}), especially at higher concentrations and/or in the presence of strong attractions or repulsions [42].

For readers unfamiliar with Eq. (1), it is a more general form for Rayleigh scattering as a function of protein concentration than the more restrictive and conventional form [42]. Unlike the more common expression, Eq. (1) is not restricted to highly dilute or weakly attractive/repulsive conditions, and is not restricted to cases where Donnan equilibria can be neglected [43]. G_{22} is a quantitative measure of protein–protein interactions that is conceptually similar to the more familiar second osmotic virial coefficient B_{22} [42], except that it carries the opposite sign as B_{22} and in the limit of low c it has double the magnitude (see also, Discussion). The reduced values ($G_{22}^* = -G_{22}/2B_{22,HS}$) are numerically equivalent to reduced B_{22} values ($B_{22}^* = B_{22}/B_{22,HS}$) in the limit of low c and/or conditions of weakly repulsive or attractive conditions; with $B_{22,HS}$ denoting the steric-only or "hard sphere" value of the second osmotic virial coefficient (see also Discussion).

The effective hard sphere or steric radius was taken as 5 nm for this IgG1, based on typical hydrodynamic radii of IgG1 antibodies [26,49]. Illustrative fits are shown in the Supporting Information (Fig. S3). The resulting G_{22}^* values are plotted as white bars in Fig. 3, corresponding to the same solvent conditions as the $T_{2\,h}$ and T_m values reported in that figure. Generally, shifts to higher pH and lower NaCl concentrations corresponded to less repulsive (less negative) G_{22}^* values. None of the conditions were strongly attractive (see also Discussion).

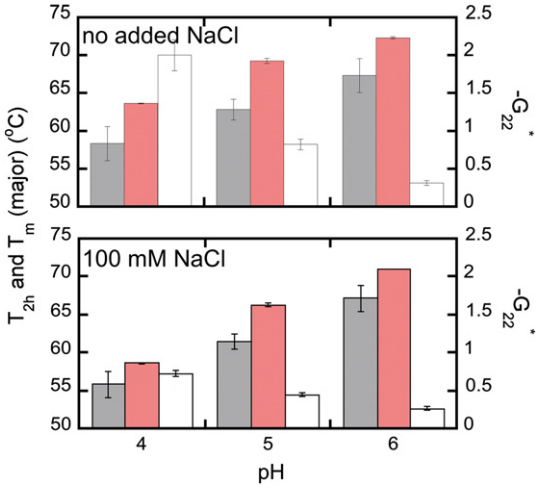

Fig. 3. Summary of pH and [NaCl] effects on aggregation rates, conformational stability, and colloidal interactions. The relative aggregation rates are represented by $T_{2\,h}$ (gray bars). Conformational stability is represented by T_m of the Fab or the major endotherm when those coincided (red bars). Colloidal interactions are represented with $-G_{22}^*$ values (white bars). The error bars are standard deviations in the replicate T_m measurements and in the nonlinear regression to determine $T_{2\,h}$ and G_{22}.

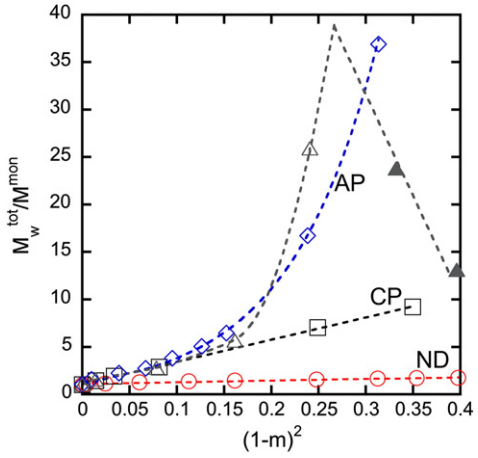

Fig. 4. Representative plots (M_w^{tot}/M^{mon} vs. $(1-m)^2$) of four aggregation mechanisms observed at different solution conditions. Red circles illustrate nucleation-dominated behavior, where aggregates formed, but did not grow greatly beyond dimers and small oligomers. Black squares show aggregate growth by rapid monomer addition (chain polymerization). Blue diamonds show aggregate growth by a combination of chain polymerization and aggregate–aggregate condensation. Gray triangles show aggregate growth by condensation as soluble species (open triangles) and eventual precipitation removing aggregates from solution (filled triangles). The dotted lines are guides to the eye.

3.4. Qualitative aggregation mechanism as function of pH and NaCl concentration

Qualitative aggregate growth mechanisms were characterized as a function of pH and NaCl concentration. The monomer fraction (SEC) and weight-average molecular weight (inline MALS) were monitored for samples incubated isothermally at accelerated conditions (elevated temperature) for slightly longer than one half-life at a given pH and [NaCl]. The initial protein concentration was 1 mg/mL, and the temperatures were selected so as to give half-lives that were of the order of hours.

Fig. S4 (Supporting information) shows representative SEC chromatograms overlaid with molecular weight information from the inline MALS for three conditions that had distinguishable aggregation growth mechanisms. Under the SEC conditions that were utilized, monomer eluted at approx. 7.9 min, dimer at approx. 6.8 min, trimer at approx. 6.3 min, and aggregates larger than trimers coeluted at approx. 5.7 min, and there was significant overlap with the trimer peak. The illustrative conditions are where: dimerization (or nucleation) dominated and any growth was slow (Fig. S4A), aggregates grew to high M_w but remained soluble and co-eluted in the void of the column (Fig. S4B), or aggregates grew large but eventually precipitated or displayed visible haze/cloudiness (Fig. S4C). The fractional conversion of monomer to aggregate (of any kind) is denoted as $1-m$, with m defined as the monomer concentration divided by its initial monomer concentration.

While it was relatively simple to identify conditions by visual inspection of SEC when aggregates remained as dimers and small oligomers, as opposed to growth to large aggregates, a different representation of the SEC–MALS data was needed to determine the mechanism by which aggregates grew while they stayed in solution. This is illustrated in Fig. 4. The weight average molecular weight, including monomers and aggregates in solution, is denoted by M_w^{tot}/M^{mon}, where the M_w^{tot} was calculated by integrating M_w across the entire chromatogram of peaks containing protein [10,11,26]. M_w^{tot} is plotted versus the square of the extent of reaction, $(1-m)^2$, in Fig. 4.

According to theoretical considerations [37,50] (see also Supplementary material), this type of plot shows linear behavior when aggregates grow primarily through monomer addition or, equivalently, chain polymerization (CP). An upturn in these types of plots represents growth of aggregates by aggregate–aggregate condensation polymerization (AP). In addition to these two growth mechanisms, the nucleation dominated (ND) regime was distinguishable as the conditions where there was a linear relationship between M_w^{tot}/M^{mon} and $(1-m)^2$, but the aggregates did not reach sizes larger than dimers and small oligomers even as one considered large extents of monomer loss (i.e., high values of $(1-m)^2$).

The gray triangles in Fig. 4 represent conditions where growth of soluble aggregates was through a hybrid mechanism: aggregate–aggregate condensation polymerization to form soluble aggregates occurred at low extents of monomer loss, but precipitation of at least the highest M_w aggregates occurred within the first two half-lives tested for Fig. 4; the solid triangles indicate samples in which visible aggregation was apparent in such longer-time samples. The final type of aggregate growth mechanism is one in which visible haze, particle formation, and/or phase separation (PS) occurred almost immediately upon detectable monomer loss. Due to the small or undetectable amounts of soluble aggregates present in such cases, it was not possible to obtain reliable M_w data from MALS for those samples, and hence and example of PS behavior is not plotted in Fig. 4.

The growth mechanism at each pH and NaCl concentration was categorized using the analysis illustrated in Fig. 4 to create a state diagram summarizing how the growth mechanism depends on pH and added NaCl. This diagram is shown in the top panel of Fig. 5. The temperature at which isothermal incubation was monitored is marked next to each of the symbols; these align semi-quantitatively with the $T_{2\,h}$ values in Fig. 2, while maximizing the number of samples that could be incubated simultaneously at the same temperature. The five types of aggregate growth mechanisms are represented by the five symbol types and the labels in Fig. 5 (see also Figure caption).

Fig. 5 shows that pH and NaCl concentrations greatly impact the growth mechanism of aggregates. At low pH, even for conditions with appreciable salt concentrations (less than approx. 200 mM), little growth occurred. At low ionic strength and pH $\ll$ pI, increasing pH first resulted in larger aggregates, growing by chain polymerization. At higher pH, aggregation resulted in visible haze almost immediately upon detectable monomer loss. At higher NaCl concentrations and low pH, aggregates were able to grow quickly to high M_w by condensation to form larger soluble aggregates. Aggregation again resulted

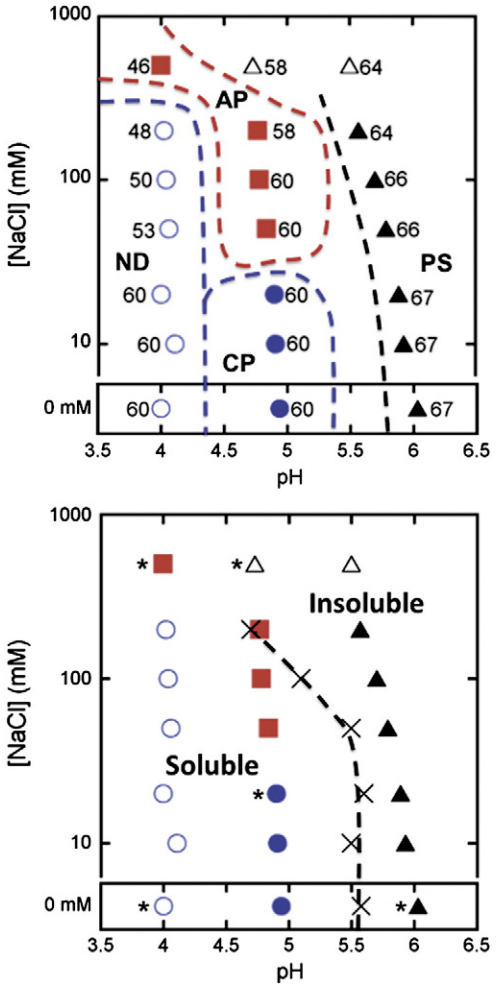

Fig. 5. [Top] State diagram of aggregation mechanisms as a function of pH and NaCl concentration. The qualitative aggregation mechanism(s) were monitored over slightly longer incubation times than the first half-life at a given temperatures (indicated by the number label next to each point in the figure). The different mechanisms are indicated by the different symbol types: nucleation dominated (open circles); growth via chain polymerization (filled circles); condensation-dominated growth (squares); condensation followed by macroscopic precipitation/phase separation (open triangles); aggregate precipitation/phase separation (filled triangles). [Bottom] Overlay of the boundary between soluble and phase-separated aggregates (X symbols and dashed line) on the state diagram of qualitative aggregation mechanisms. See main text for additional details. Structural analyses of the resulting aggregates were performed at conditions indicated with asterisks, corresponding to the conditions for Fig. 7.

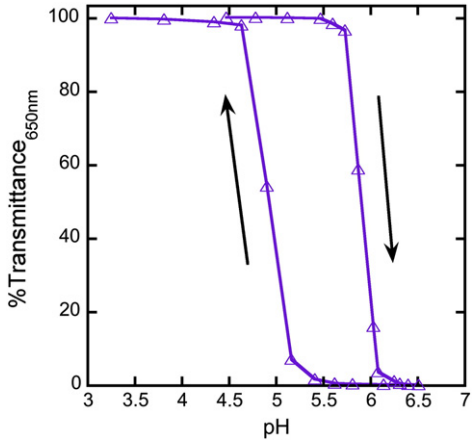

Fig. 6. Illustrative pH titration at room temperature of initially soluble aggregates, prepared as described in Materials and methods. The aggregate concentration was slightly higher (0.9 mg/mL, with 0.1 mg/mL residual monomer) to make the transition more visibly pronounced for clarity in the figure. The percent transmittance at 650 nm was used as a measure of turbidity at each pH step in the titration. The dashed lines are guides to the eye for identifying the inflection point as the nominal cloud point.

in visibly hazy and particulate suspensions at sufficiently high pH (but still well below the pI). In general, addition of NaCl and/or increased pH led to enhanced aggregate–aggregate coalescence (AP or PS mechanisms).

3.5. Reversible aggregate phase separation

Previous studies [26,28] indicated that a reversible phase transition can occur for non-native aggregates (rather than monomers), and that this may explain the pH and salt dependence of the formation of haze and macroscopic particles. In order to test this hypothesis for anti-SA IgG1 aggregates, pH titrations were performed on initially soluble aggregates under conditions corresponding to the pH and [NaCl] ranges in Fig. 5, with solutions that contained 50:50 aggregate: monomer (by mass). This corresponding to samples incubated at elevated temperatures for 1 half-life, in keeping with the behavior categorized in the state diagram in Fig. 5.

Fig. 6 shows a representative pH titration of an initially soluble aggregate sample. As pH was raised, the aggregates phase separated to form white visible haze (not shown). Then, as the pH was lowered on the same sample, the suspension dissolved to form a clear solution. SEC before and after the pH titration showed no change in monomer content. If the sample was centrifuged prior to lowering the pH to dissolve the particles, they sedimented readily and the supernatant was transparent (not shown).The curves in Fig. 6 indicate that there is a hysteresis effect, in that the forward and reverse pH titrations do not overlay in the transition region. This is expected based on previous studies [26,28] in which it was found that if one performed titrations over much longer time scales – of the order of hours to days for each step in pH along the curve – then the two curves overlapped. In the present case, samples were only held for ~1 min at each pH, but the curves were reproducible upon cycling up and down in pH (not shown).

Monomer controls at the same concentration remained transparent (100% transmission) in all cases, showing that this transition is due to the aggregates, not an underlying monomer transition. This indicates that the formation of a suspension of visible or large subvisible particles is, at least in part, a result of reversible phase separation of aggregates; as seen previously for aCgn and for other antibodies [26,28,29]. The pH value at which the initial down turn in % transmission occurred (i.e., the nominal cloud point) was determined at a series of NaCl concentrations. These cloud points are shown as X symbols, connected by a dotted line, in the bottom panel of Fig. 5, to show where this cloud point boundary lies on the aggregation state diagram for anti-SA IgG1.

3.6. Structural changes with aggregation

Structural changes accompanying aggregation were characterized at five conditions corresponding to the five growth mechanisms, using a combination of spectroscopic techniques that probe secondary structure and/or different measures of tertiary structure, relative to the folded monomer. The conditions chosen for characterization are marked with asterisks in the bottom panel of Fig. 5, corresponding to state points that lie within each of the five regimes in the state diagram. These are also summarized in Table S1 (Supporting information).

Solution conditions where the aggregates did not essentially all precipitate were tested using far-UV CD, intrinsic fluorescence, and ThT binding. Fig. 7A shows the corresponding spectra after the contribution from residual monomer was subtracted (see Materials and methods). For clarity, the monomer spectrum is shown for comparison to the aggregate spectra in Figs. 7B and 7C show analogous results

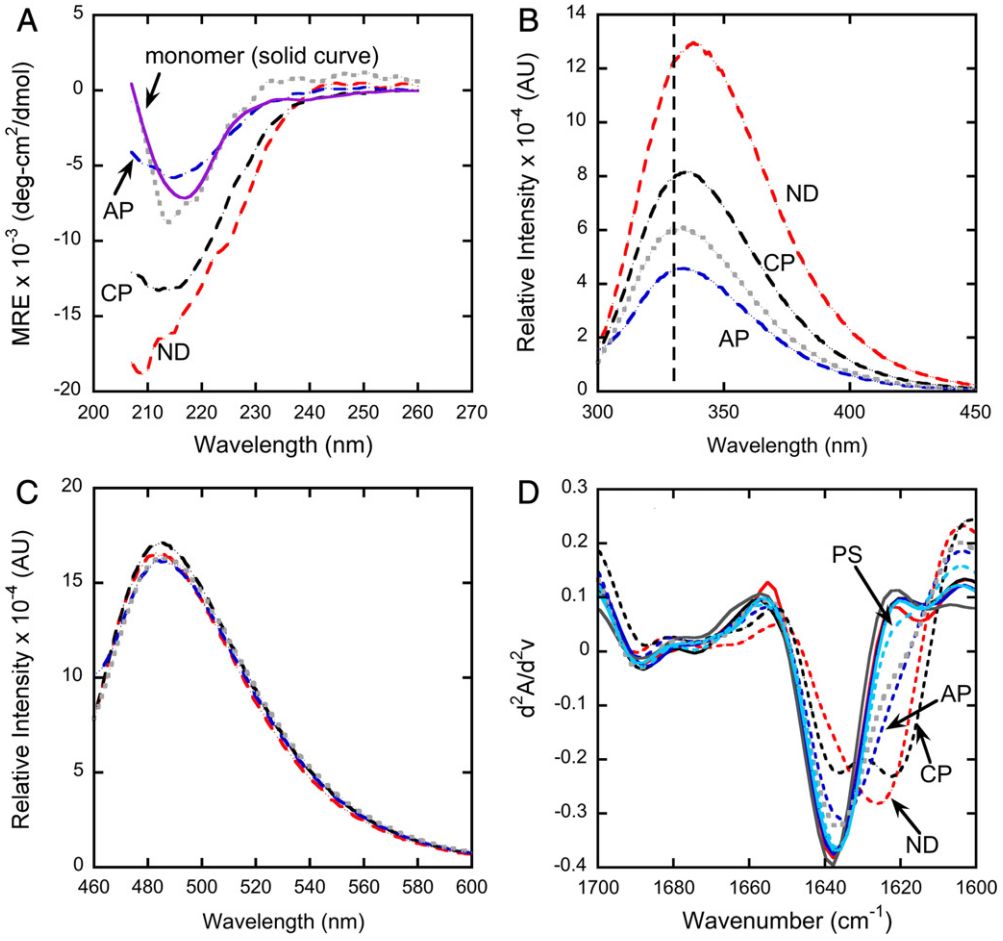

Fig. 7. (A) Far-UV circular dichroism (CD) spectra for aggregates at five different conditions corresponding to different regions of the aggregation mechanism state diagram. Spectra for aggregates are shown with monomer contributions subtracted from the corresponding full spectrum. The solid line is the average of the monomer spectra, included for reference. Red dashed: nucleation dominated; black dashed: growth by chain polymerization; blue dashed: growth primarily by condensation; gray dotted: growth by condensation and then precipitation (unlabeled in figure). (B) Akin to panel A, but for intrinsic fluorescence spectra (no monomer spectrum shown); monomer peak position was essentially independent of pH and [NaCl] (value indicated by the vertical dashed line), peak height increased from 4×10^4 (pH 4) to 4.7×10^4 (pH 5) to 5.6×10^4 (pH 6), and was only weakly dependent on [NaCl]. (C) Akin to panels A and B, but for Thioflavin T fluorescence upon binding to aggregates; monomers did not show appreciable binding (D) FTIR spectra analogous to panel A, but also including the condition where haze and precipitates/phase-separation dominated. Solid curves are the monomer spectra, which are essentially independent of solvent condition.

for intrinsic fluorescence and ThT binding, respectively. Monomer does not appreciably bind ThT relative to buffer controls (not shown).The corresponding monomer spectra are not shown in Fig. 7B for visual clarity. The peak maximum for monomer was at 330 nm (indicated by a vertical dashed line in Fig. 7B). In each case, there was a red shift in the peak position for the aggregates compared to monomer, and the fluorescence intensity was greater (per unit mass) than that of monomer. Fig. 7D shows Amide I FTIR spectra for aggregated samples (mixture of aggregate and monomer) for each of the conditions in Table S1, as well as the monomer controls. Monomer spectra were indistinguishable from one another for the range of conditions tested. These include the conditions in panels A to C, but also include the PS condition since FTIR is unaffected by scattering artifacts that otherwise preclude the use of the spectroscopies needed for panels A to C.

In terms of CD, the aggregates that grew by nucleation dominated (ND) and chain polymerization (CP) mechanisms appeared to have the largest changes in their secondary structure; the negative peak at around 217 nm increased in intensity and width, with a slight blue shift. The conditions where growth was dominated by aggregate–aggregate condensation polymerization, whether the aggregates remained in solution or eventually phase separated, appeared to have relatively smaller changes in secondary structure compared to monomer. As noted above, there were no discernable changes in monomer spectra over the pH and salt conditions tested.

In terms of intrinsic FL, aggregation resulted in larger intensities and red shifts in the emission spectra, regardless of growth mechanism. This corresponds to greater solvent exposure for at least some Trp residues, and possibly some quenching of Trp fluorescence in the folded monomer state, as observed before for aggregation of a different IgG1 antibody, as well as for globular proteins [10,38]. Aggregation at low pH and low [NaCl] (i.e., ND conditions) resulted in the largest detected change in Trp exposure, followed by slightly higher pH and NaCl concentration (CP conditions), and finally the smallest detectable changes at higher pH and/or NaCl concentration (AP and AP + PS conditions).

ThT binding monitored by fluorescence emission for the same sample conditions showed aggregated samples bound ThT strongly. However, unlike the CD and intrinsic FL, the bound spectra are virtually indistinguishable. From the FTIR second derivative spectra of the amide I, it was apparent that all but one condition of the aggregated samples showed a shift from about 1640 cm^{-1} to ~1620 cm^{-1} (negative peaks), indicative of major beta-sheet alteration. For the exception (PS), there was little alteration in structure. The CP aggregates seemed to indicate either a partial or two different populations of beta-sheet aggregates with negative peaks at approximately 1640 cm^{-1}

and 1620 cm^{-1}. Subtle changes in turn structure (~1660 cm^{-1} to 1680 cm^{-1}) accompanied these major alterations in beta-sheet structure.

4. Discussion

4.1. Aggregation rates show opposite correlations with T_m and G_{22} vs. pH and [NaCl]

Increasing pH and adding NaCl had significant effects on the conformational transitions observed in DSC. With increasing pH, T_m values of all discernable endotherms shifted to higher temperatures, indicating increased conformational stability of multiple domains. This occurred both with and without added NaCl, but transitions occurred at systematically lower T_m values with 100 mM NaCl present for a given pH. For pH 4 conditions, this resulted in a more distinguished C_H2 peak. In this case, it was possible to discern more than one endotherm, and the largest-area endotherm corresponded to the onset of aggregation during repeated heating; suggesting Fab unfolding was involved with aggregate formation under those conditions. This was also consistent with previous results for a series of different IgG1 antibodies [10,11,27].At higher pH values, only one main endotherm was unambiguously discernable. At these conditions, it is hypothesized that unfolding of multiple domains occurred simultaneously; this includes the aggregation-prone region(s), as that single endotherm was not significantly reversible.

The value of $G_{22}{}^*$ is a measure of net colloidal interactions, such as hydrophobic, van der Waals, and electrostatic interactions. Any value of $-G_{22}{}^*$ above 1 indicates net repulsive interactions that are greater than those based solely on steric interactions, and this is typically due to electrostatic repulsions. Any value below 1 indicates net attractions relative to steric-only interactions, and may be due to a combination of electrostatic and non-electrostatic contributions.

Upon increasing pH with pH ≪ pI (~9), there was a significant decrease in $-G_{22}{}^*$ both with and without added salt for anti-SA IgG1. At the lowest pH and ionic strength conditions, $-G_{22}{}^*$ was significantly greater than 1, indicating electrostatic repulsions were prominent. At higher pH, or with 100 mM of added NaCl at all pH values, $-G_{22}{}^*$ was below 1; indicating reduced, but not necessarily negligible electrostatic repulsions, and effectively net attractions relative to steric-only interactions. The effects of added NaCl were most pronounced at low pH, and became effectively negligible aspH increased towards the pI, while still approximately 3 units below the pI. The salt dependence is consistent with strong electrostatic, repulsive interactions at low pH, with weak or negligible contributions from electrostatic repulsions or attractions at higher pH values, consistent with a large reduction in net charge on the protein surface as acidic residues become charged to counterbalance the charged basic residues.

In comparing the effects of pH and added NaCl on conformational stability (T_m), colloidal interactions ($-G_{22}{}^*$), and relative aggregation rates ($T_{2\,h}$), it is apparent that aggregation rate is strongly related to conformational stability. The difference between $T_{2\,h}$ and T_m was relatively constant among the six conditions examined. This is apparent both from inspection of Fig. 3, and by plotting $T_{2\,h}$ versus T_m (Fig. S5, Supporting information). Higher $T_{2\,h}$ values indicate relatively lower aggregation rates if one were to consider a common $T<T_{2\,h}$, and this correlates quantitatively with increased conformational stability for anti-SA IgG1 as a function of pH and [NaCl]. Fig. 3 clearly shows that the opposite trend occurs when comparing $T_{2\,h}$ and colloidal interactions ($G_{22}{}^*$). That is, as $T_{2\,h}$ rises (lower relative aggregation rates) the colloidal interactions become increasingly attractive; this is the opposite of what one anticipates if colloidal interactions were a strong determinant of aggregation rates [16,22,51].

From a mechanistic perspective, this suggests that the decrease in concentration of (partially) unfolded monomers, due to increased Fab T_m values, more than offsets the more attractive colloidal interactions as pH is increased for anti-SA IgG1. There is also a small increase in aggregation rates (decreased $T_{2\,h}$) with increasing [NaCl] at fixed pH, but this is a much less pronounced effect except at low pH. In that case, added NaCl does cause a large drop in colloidal repulsions, and this may help to explain the increased aggregation rates. This illustrates the importance of simultaneously investigating multiple factors that may determine relative aggregation rates [22], because different conclusions would have been drawn if only ionic strength was varied at pH 4. As such, it appears that conformational stability is a dominant factor controlling aggregation rates for anti-SA IgG1 under most of the conditions considered here, with the exception being conditions of strong electrostatic repulsions.

4.2. pH and [NaCl] effects on aggregation mechanism and formation of insoluble aggregates

The state diagram in Fig. 6 indicates that aggregate growth mechanism is strongly dependent on pH and [NaCl] at these acidic conditions. At low pH and NaCl concentrations, high net charge of the protein monomers and minimal shielding of these charges result in large inter-molecular repulsions. The strongly repulsive electrostatic interactions resulted in the large repulsive $-G_{22}{}^*$ value observed at pH 4, 0 mM NaCl, as discussed above. This solution condition also produced aggregates via nucleation dominated (ND) growth, where aggregates formed (i.e., "nucleated" as dimers) but did not grow to a large extent; although dimers did grow slowly to trimers and at least tetramers, so it is not reasonable to conclude that dimers were completely incapable of growth. The strong electrostatic repulsions between monomers and aggregates (dimers, etc.) and between aggregates themselves may provide an explanation for the lack of CP, AP, or PS under these conditions, and this would be consistent with the lack of AP or PS mechanisms for a different IgG [10] or for alpha-chymotrypsinogen A under similar solvent conditions and elevated temperature [24].

Moving higher in pH and NaCl concentrations, results in appreciable growth, and thus larger aggregates. Increasing pH towards the pI (~9) results in lower electrostatic repulsions as the net charge on the protein decreases. In addition, increasing pH increases the buffer-salt ionic strength, which shields the net charge of the molecules, resulting in lower inter-molecular repulsions. Increasing NaCl concentration also results in lower electrostatic repulsions via decreased charge shielding. This further supports the conclusion that electrostatic repulsions (or lack thereof) are important determinants of aggregate growth mechanisms.

Overlaying the phase and state diagrams in the bottom panel of Fig. 6 suggests that the kinetics and thermodynamics of forming of insoluble aggregates are by the same or similar mechanisms. From the state diagram alone, it appears that beyond a certain regime of pH–[NaCl] condition the condensation of aggregates was rapid enough for the formation of visible particles. A similar conclusion is reached by comparison with the cloud-point boundary. An overlap of the cloud-point boundary and the shift from soluble to insoluble aggregates during kinetic measurements was also recently reported in detail for aCgn aggregates [28], and much less systematically for a different IgG1 antibody over a similar pH range [10]. This suggests that the formation of visible particles upon storage or during accelerated kinetic tests may be due to a phase separation driven by rapid condensation of aggregates, and this may be driven by electrostatic effects that are akin to those in more well-studied colloidal or polyelectrolyte systems [28].

4.3. Structural changes during aggregation and possible relation to the mechanism of aggregation

The assays used here report on changes in the average structure of proteins that comprise aggregates — that is, they report on both

misfolded and folded structure simultaneously. The possible exception to this is ThT binding, as the binding to native or native-like configurations is dramatically less than that for amyloid-like or similar beta-sheet structure. It is not clear from the present results whether the structural differences in the aggregates reported by FTIR, CD, or intrinsic FL are relevant with regard to the observed differences in the growth mechanisms. Qualitatively, conditions with larger electrostatic repulsions between monomers (based on G_{22}*) correlate to some degree with the larger degrees of secondary and tertiary structure change upon aggregation. One hypothesis that may explain this is that such conditions also have the greatest electrostatic repulsion between amino acids within a given a protein chain, making larger conformational changes (involving multiple regions of the protein) more favorable than in conditions of weaker electrostatic repulsion. Interestingly, there were no distinguishable differences in the unheated monomer samples at different solvent conditions, so this effect presumably was manifest as part of the aggregation process and was not intrinsic to the folded monomer state.

Given the changes in the bulk spectroscopic signals, the lack of difference in the ThT spectra is rather striking. One interpretation is that if the dye is binding to the key "hot spots" that make up strong stabilizing inter-protein contacts in the aggregates, then the other structural changes detected in FTIR, CD, and intrinsic FL might not be tied strongly to the mechanism(s) by which monomers are converted to aggregates. That is, one can envision a scenario where different regions of secondary structure of the protein unfold to a greater extent at lower pH and ionic strength, prior to aggregate formation. However, if only certain sequence "hot spots" are the key contacts between monomers in the aggregates, then only the structural perturbations that reveal those "hot spots" may be relevant to promoting aggregate formation. The smaller perturbations observed at higher pH and ionic strength may simply reflect that smaller structural perturbations are needed in terms of revealing "hot spots" if monomer–monomer charge repulsions are weaker, and therefore monomers inherently can more easily come together. In that case, the differences in overall unfolded structure observed in the bulk spectroscopies may be misleading in addressing the question of whether an observed structural change is directly relevant in the aggregation process — this is likely more so the case for large multi-domain proteins such as antibodies, where unfolding of only certain domains may be an "on pathway" step in aggregation.

However, as the exact mechanism and location(s) of ThT binding are unclear, an alternative hypothesis is that ThT binding reports on only one aspect of the relevant structural change(s) – e.g., forming only one type of key monomer–monomer contacts – while CD, intrinsic FL, and FTIR are capturing other important structural details. For example, there may be multiple "hot spots" that could form stabilizing inter-protein contacts, and different structural perturbations that occur preferentially at different solution conditions then lead to aggregates with different degrees of unfolding in the constituent monomers. This would then require that ThT is binding to different aggregate structures relatively indiscriminately, which is counter to its historical use as an amyloid-specific dye [5,18]. The present data cannot resolve these possible interpretations, and to do so will likely require higher resolution assays that are sensitive to local conformational differences, for example HDX-MS with partial proteolysis. Such an approach was useful in previous work (Ref. [32] and references therein) using reporter peptides to show which small regions of a given protein were buried from solvent upon aggregation.

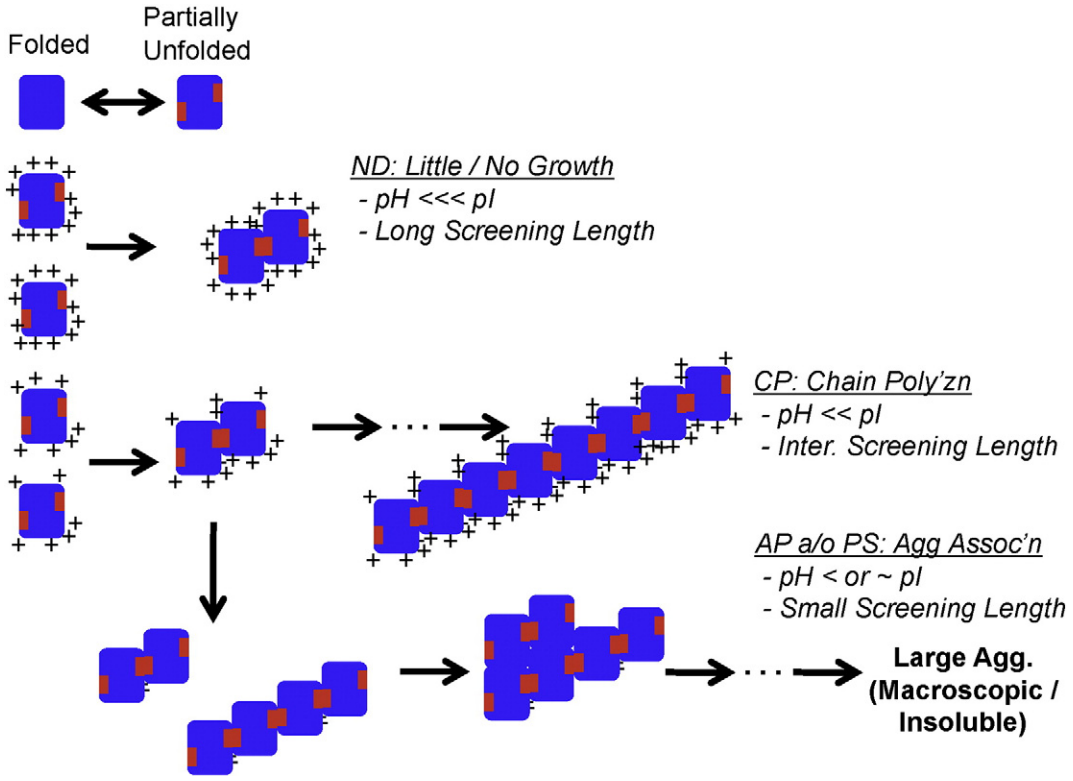

Fig. 8. Schematic summary of the hypothesized role of interactions between aggregates, compared to those between monomers or monomers and aggregates, highlighting that both non-specific colloidal interactions (charge–charge interactions, hydrophobic and/or van der Waals) and more specific sequence-dependent interactions (indicated in red) are important in the different processes of non-native protein aggregation. As pH and/or salt concentration are changed, electrostatic repulsions are reduced, net charge and screening length are reduced, allowing more non-specific attractions between aggregates to dominate over the specific monomer–monomer and monomer–aggregate interactions. For simplicity of representation, only net positive net charges shown for this example with pH<pI, with titration to introduce compensatory negative charges understood as pH is increased. Equivalent arguments hold for acidic proteins with pH>pI, as pH is decreased towards the pI.

4.4. In vitro global aggregation behavior of related proteins

Overall, the global aggregation behavior anti-SA IgG1 is consistent with observations in more limited studies for other IgG1 and IgG2 antibodies, as well as more globular proteins from a variety of structural classes, as a function of pH and ionic strength, in that pH and ionic strength play a dominant role in determining which aggregate growth pathway(s) will be followed [10,11,13,18,24,26,27,29]. This argument is further supported by a recent systematic study of the aggregate growth kinetics for IgG antibodies over a range of pH and salt conditions, in which a common quantitative scaling behavior held for a wide variety of conditions [54,55]. These results suggest that while the specific amino-acid "hot spots" within a protein sequence will differ for different proteins, once aggregates (or nuclei) are initially formed their subsequent growth pathway(s) may be more generally understood by considered relatively non-specific mechanisms based on colloid physics. Physically, this may occur because the process of "nuclei" formation inherently may bury specific "hotspots" by forming strong protein–protein interfaces (e.g., as in the schematic in Fig. 8). The interactions between aggregates – as opposed to monomers – as they self-associate could then be based primarily on non-specific interactions such as colloidal electrostatic repulsions/attractions and hydrophobic/dispersive attractions. In Fig. 8, the latter process is the self-association of aggregates in the AP, AP + PS, or PS mechanism, while the former is depicted with the red "hotspots" becoming strongly correlated between monomers and other monomers, or monomer and chain polymers with which they strongly bind. Future work will test this hypothesis by considering how well the global aggregation behavior of this and other proteins can be predicted based on simple biophysical models that build upon this premise.

Interestingly, all aggregates of anti-SA IgG1 displayed quantitatively similar, strong ThT binding, suggesting a common underlying structure in terms of amyloid-like non-native structure for at least a portion of the molecule. This is similar to observations for a different IgG1 that aggregated with concomitant Fab unfolding [10], and this potentially provides support for the use of amyloid-based "aggregation calculators" in attempting to predict hot-spots for targeting with antibody-engineering strategies [52]. Interestingly, only Fc unfolding is implicated in aggregation of some IgG1 antibodies if one considers much lower pH than was tested here [53], and therefore it is also possible that the role of Fab unfolding in the aggregation process may depend on the solution conditions of interest. As noted above, given that multiple "hot spots" are likely present in large, multi-domain proteins such as monoclonal antibodies [52], it is likely that different nucleation pathways or key intermediates may be possible. As such, while growth pathways may be amenable to treatments based on non-specific colloidal interactions, it appears more likely that the initiation or nucleation processes will be more protein specific and more challenging to treat with non-specific models based on colloidal and homopolymer biophysical treatments.

5. Summary and conclusions

This report describes a global study on the aggregation of a model IgG1 as a function of pH and [NaCl]. Both of these variables were found to strongly influence aggregation rates, mechanisms of aggregate growth, aggregate phase behavior, and the average secondary/tertiary structure of the resulting aggregates. Varying pH and [NaCl] resulted in changes in conformational stability and inter-molecular colloidal interactions that were opposite to one another in most cases. Aggregate growth mechanisms, and phase behavior of aggregates were sensitive to electrostatic repulsions, with an aggregate–aggregate phase transition that semi-quantitatively aligned with conditions that produced visibly aggregated samples upon accelerated storage. Although different structural features were apparent for aggregates from different solution conditions, in all cases the aggregates bound ThT in a quantitatively and qualitatively similar fashion, suggesting a common set of underlying structures or interactions, possibly amyloid in nature, and involving Fab unfolding as a key step in non-native aggregate formation. The results suggest that growth mechanisms may be amenable to interpretation based on relatively non-specific, colloidal models.

Acknowledgments

The National Science Foundation (CBET-0931173) is gratefully acknowledged for financial support. P. Arosio and M. Morbidelli are thanked for bringing references [54] and [55] to our attention.

Appendix A. Supplementary data

Supplementary data to this article can be found online at http://dx.doi.org/10.1016/j.bpc.2012.12.004.

References

[1] W. Wang, S. Singh, D.L. Zeng, K. King, S. Nema, Antibody structure, instability, and formulation, Journal of Pharmaceutical Sciences 96 (2007) 1–26.
[2] P. Chames, M. Van Regenmortel, E. Weiss, D. Baty, Therapeutic antibodies: successes, limitations and hopes for the future, British Journal of Pharmacology 157 (2009) 220–233.
[3] W. Wei, Protein aggregation and its inhibition in biopharmaceutics, International Journal of Pharmaceutics 289 (2005) 1–30.
[4] H. Mahler, W. Friess, U. Grauschopf, S. Kiese, Protein aggregation: pathways, induction factors and analysis, Journal of Pharmaceutical Sciences 98 (2009) 2909–2934.
[5] W.F. Weiss IV, T.M. Young, C.J. Roberts, Principles, approaches, and challenges for predicting protein aggregation rates and shelf life, Journal of Pharmaceutical Sciences 98 (2009) 1246–1277.
[6] A.S. Rosenberg, Effects of protein aggregates: an immunologic perspective, The AAPS Journal 8 (2006) E501–E507.
[7] S. Hermeling, D.J.A. Crommelin, H. Schellekens, W. Jiskoot, Structure–immunogenicity relationships of therapeutic proteins, Pharmaceutical Research 21 (2004) 897–903.
[8] A. Braun, L. Kwee, M.A. Labow, J. Alsenz, Protein aggregates seem to play a key role among the parameters influencing the antigenicity of interferon alpha (IFN-α) in normal and transgenic mice, Pharmaceutical Research 14 (1997) 1472–1478.
[9] H. Schellekens, Factors influencing the immunogenicity of therapeutic proteins, Nephrology, Dialysis, Transplantation 20 (2005) vi3–vi9.
[10] R.K. Brummitt, D.P. Nesta, L. Chang, S.F. Chase, T.M. Laue, C.J. Roberts, Nonnative aggregation of an IgG1 antibody in acidic conditions: Part 1. Unfolding, colloidal interactions, and formation of high-molecular-weight aggregates, Journal of Pharmaceutical Sciences 100 (2011) 2087–2103.
[11] E. Sahin, A.O. Grillo, M.D. Perkins, C.J. Roberts, Comparative effects of pH and ionic strength on protein–protein interactions, unfolding, and aggregation for IgG1 antibodies, Journal of Pharmaceutical Sciences 99 (2010) 4830–4848.
[12] S.R. Brych, et al., Characterization of antibody aggregation: role of buried, unpaired cysteines in particle formation, Journal of Pharmaceutical Sciences 99 (2010) 764–781.
[13] A.W.P. Vermeer, W. Norde, The thermal stability of immunoglobulin: unfolding and aggregation of a multi-domain protein, Biophysical Journal 78 (2000) 394–404.
[14] L.F. Anthony, Protein aggregation: folding aggregates, inclusion bodies and amyloid, Folding & Design 3 (1998) R9–R23.
[15] S. Krishnan, E.Y. Chi, J.N. Webb, B.S. Chang, D. Shan, M. Goldenberg, M.C. Manning, T.W. Randolph, J.F. Carpenter, Aggregation of granulocyte colony stimulating factor under physiological conditions: characterization and thermodynamic inhibition, Biochemistry 41 (2002) 6422–6431.
[16] E.Y. Chi, S. Krishnan, T.W. Randolph, J.F. Carpenter, Physical stability of proteins in aqueous solution: mechanism and driving forces in nonnative protein aggregation, Pharmaceutical Research 20 (2003) 1325–1336.
[17] C.J. Roberts, Non-native protein aggregation kinetics, Biotechnology and Bioengineering 98 (2007) 927–938.
[18] M.R.H. Krebs, G.L. Devlin, A.M. Donald, Amyloid fibril-like structure underlies the aggregate structure across the pH range for β-lactoglobulin, Biophysical Journal 96 (2009) 5013–5019.
[19] B.S. Kendrick, J.L. Cleland, X. Lam, T. Nguyen, T.W. Randolph, M.C. Manning, J.F. Carpenter, Aggregation of recombinant human interferon gamma: kinetics and structural transitions, Journal of Pharmaceutical Sciences 87 (1998) 1069–1076.
[20] A.O. Grillo, K.L. Edwards, K.S. Kashi, K.M. Shipley, L. Hu, M.J. Besman, C.R. Middaugh, Conformational origin of the aggregation of recombinant human factor VIII, Biochemistry 40 (2000) 586–595.
[21] D.S. Goldberg, S.M. Bishop, A.U. Shah, H.A. Sathish, Formulation development of therapeutic monoclonal antibodies using high-throughput fluorescence and static light scattering techniques: role of conformational and colloidal stability, Journal of Pharmaceutical Sciences 100 (2011) 1306–1315.

[22] C.J. Roberts, T.K. Das, E. Sahin, Predicting solution aggregation rates for therapeutic proteins: approaches and challenges, International Journal of Pharmaceutics 418 (2011) 318–333.
[23] F. He, C.E. Woods, G.W. Becker, L.O. Narhi, V.I. Razinkov, High-throughput assessment of thermal and colloidal stability parameters for monoclonal antibody formulations, Journal of Pharmaceutical Sciences 100 (2011) 5126–5141.
[24] Y. Li, B.A. Ogunnaike, C.J. Roberts, Multi-variate approach to global protein aggregation behavior and kinetics: effects of pH, NaCl, and temperature for α-chymotrypsinogen A, Journal of Pharmaceutical Sciences 99 (2010) 645–662.
[25] W. Hoyer, T. Antony, D. Cherny, G. Heim, T.M. Jovin, V. Subraniam, Dependence of α-synuclein aggregate morphology on solution conditions, Journal of Molecular Biology 322 (2002) 383–393.
[26] R.K. Brummitt, D.P. Nesta, L. Chang, A.M. Kroetsch, C.J. Roberts, Nonnative aggregation of an IgG1 antibody in acidic conditions, Part 2: nucleation and growth kinetics with competing growth mechanisms, Journal of Pharmaceutical Sciences 100 (2011) 2104–2119.
[27] Y. Li, H. Mach, J.T. Blue, High throughput formulation screening for global aggregation behaviors of three monoclonal antibodies, Journal of Pharmaceutical Sciences 100 (2011) 2120–2135.
[28] A.M. Kroetsch, E. Sahin, H.-Y. Wang, C.J. Roberts, Phase behavior of amyloid polymers of alpha-chymotrypsinogen, A Journal of Pharmaceutical Sciences 101 (2012) 3651–3660.
[29] E. Sahin, W.F. Weiss IV, A.M. Kroetsch, K.R. King, R.K. Kessler, T.K. Das, C.J. Roberts, Aggregation and pH–temperature phase behavior for aggregates of an IgG2 antibody, Journal of Pharmaceutical Sciences Sciences 101 (2012) 1678–1687.
[30] J.L. Fast, A.A. Cordes, J.F. Carpenter, T.W. Randolph, Physical instability of a therapeutic Fc fusion protein: domain contributions to conformational and colloidal stability, Biochemistry 48 (2009) 11724–11736.
[31] C.B. Andersen, M. Manno, C. Rischel, M. Thórólfsson, V. Martorana, Aggregation of a multidomain protein: a coagulation mechanism governs aggregation of a model IgG1 antibody under weak thermal stress, Protein Science 19 (2010) 279–290.
[32] A. Zhang, S.K. Singh, M.R. Shirts, S. Kumar, E.J. Fernandez, Distinct aggregation mechanisms of monoclonal antibody under thermal and freeze–thaw stresses revealed by hydrogen exchange, Pharmaceutical Research 29 (2011) 236–250.
[33] H. Franey, S.R. Brych, C.G. Kolvenbach, R.S. Rajan, Increased aggregation propensity of IgG2 subclass over IgG1: role of conformational changes and covalent character in isolated aggregates, Protein Science 19 (2010) 1601–1615.
[34] J.S. Bee, M. Davis, E. Freund, J.F. Carpenter, T.W. Randolph, Aggregation of a monoclonal antibody induced by adsorption to stainless steel, Biotechnology and Bioengineering 105 (2010) 121–129.
[35] R. Thirumangalathu, S. Krishnan, M.S. Ricci, D.N. Brems, T.W. Randolph, J.F. Carpenter, Silicone oil- and agitation-induced aggregation of a monoclonal antibody in aqueous solution, Journal of Pharmaceutical Sciences 98 (2009) 3167–3181.
[36] Y. Li, W.F. Weiss IV, C.J. Roberts, Characterization of high-molecular-weight nonnative aggregates and aggregation kinetics by size exclusion chromatography with inline multi-angle laser light scattering, Journal of Pharmaceutical Sciences 98 (2009) 3997–4016.
[37] E. Sahin, C.J. Roberts, Therapeutic proteins: methods and protocols, Second Ed., (Methods in Molecular Biology series). Springer, Humana Press, 2012.
[38] J.M. Andrews, C.J. Roberts, Non-native aggregation of α-chymotrypsinogen occurs through nucleation and growth with competing nucleus sizes and negative activation energies†, Biochemistry 46 (2007) 7558–7571.
[39] P.L. Privalov, Stability of proteins: small globular proteins, Advances in Protein Chemistry 33 (1979) 167–241.
[40] R.K. Brummitt, D.P. Nesta, C.J. Roberts, Predicting accelerated aggregation rates for monoclonal antibody formulations, and challenges for low-temperature predictions, Journal of Pharmaceutical Sciences 100 (2011) 4234–4243.
[41] C.P. Winsor, The Gompertz curve as a growth curve, Proceedings of the National Academy of Sciences of the United States of America 18 (1932) 1–8.
[42] M.A. Blanco, E. Sahin, Y. Li, C.J. Roberts, Reexamining protein–protein and protein–solvent interactions from Kirkwood–Buff analysis of light scattering in multicomponent solutions, The Journal of Chemical Physics 134 (2011), (225103-225103-12).
[43] D. Asthagiri, A. Paliwal, D. Abras, A.M. Lenhoff, M.E. Paulaitis, A consistent experimental and modeling approach to light-scattering studies of protein–protein interactions in solution, Biophysical Journal 88 (2005) 3300–3309.
[44] E. Garber, S.J. Demarest, A broad range of Fab stabilities within a host of therapeutic IgGs, Biochemical and Biophysical Research Communications 355 (2007) 751–757.
[45] R.M. Ionescu, J. Vlasak, C. Price, M. Kirchmeier, Contribution of variable domains to the stability of humanized IgG1 monoclonal antibodies, Journal of Pharmaceutical Sciences 97 (2008) 1414–1426.
[46] R.L. Remmele, S.D. Bhat, D.H. Phan, W.R. Gombotz, Minimization of recombinant human Flt3 ligand aggregation at the T_m plateau: a matter of thermal reversibility, Biochemistry 38 (1999) 5241–5247.
[47] A. Ginsburg, Reversible, thermally induced domain unfolding in oligomeric proteins. Spectral and DSC measurements, Journal of Thermal Analysis and Calorimetry 61 (2000) 425–436.
[48] B.A. Ogunnaike, Random Phenomena: Fundamentals of Probability and Statistics for Engineers, CRC Press, 2009.
[49] S. Yadav, S.J. Shire, D.S. Kalonia, Factors affecting the viscosity in high concentration solutions of different monoclonal antibodies, Journal of Pharmaceutical Sciences 99 (2010) 4812–4829.
[50] Y. Li, C.J. Roberts, Lumry–Eyring nucleated-polymerization model of protein aggregation kinetics. 2. Competing growth via condensation and chain polymerization, The Journal of Physical Chemistry B113 (2009) 7020–7032.
[51] V. Kumar, N. Dixit, L. (Lisa) Zhou, W. Fraunhofer, Impact of short range hydrophobic interactions and long range electrostatic forces on the aggregation kinetics of a monoclonal antibody and a dual-variable domain immunoglobulin at low and high concentrations, International Journal of Pharmaceutics 421 (2011) 82–93.
[52] X. Wang, T.K. Das, S.K. Singh, S. Kumar, Potential aggregation prone regions in biotherapeutics: a survey of commercial monoclonal antibodies, MAbs 1 (2009) 254–267.
[53] S.B. Hari, H. Lau, V. Razinkov, S. Chen, R. Latypov, Acid-induced aggregation of human monoclonal IgG1 and IgG2: molecular mechanism and the effect of solution composition, Biochemistry 49 (2010) 9328–9338.
[54] P. Arosio, B. Jaquet, H. Wu, M. Morbidelli, On the role of salt type and concentration on the stability behavior of a monoclonal antibody solution, Biophysical Chemistry 168–169 (2012) 19–27.
[55] P. Arosio, S. Rima, M. Lattuada, M. Morbidelli, Population balance modeling of antibody aggregation kinetics, The Journal of Physical Chemistry B116 (2012) 7066–7075.